

# OSPO: Object-Centric Self-Improving Preference Optimization for Text-to-Image Generation

Yoonjin Oh, Yongjin Kim, Hyomin Kim, Donghwan Chi, Sungwoong Kim\*

Korea University

{dhdbsrcw, rla020, khmiec, zheedong, swkim01}@korea.ac.kr

## Abstract

Recent advances in Multimodal Large Language Models (MLLMs) have enabled models to perform both understanding and generation of multimodal data in a unified manner. However, achieving a fine-grained alignment between input prompts and generated images remains a major challenge especially in text-to-image generation. Therefore, recent works have introduced self-improving mechanisms based on self-generated data and self-feedback to efficiently mitigate this challenge without relying on external large-scale data or models. However, existing self-improving approaches have not focused on fine-grained visual details especially at the object level in generating training data or providing a feedback, and thus they still struggle to resolve the object hallucination problem in text-to-image generation. To tackle this problem, we propose Object-centric Self-improving Preference Optimization (OSPO), a self-improving framework for enhancing object-level text-image alignment. OSPO is designed to explicitly address the need for constructing and leveraging object-level hard negative data and an object-centric optimization in improving object-specific fidelity. In specific, OSPO consists of: (1) Initial Prompt Generation (2) Hard Preference Pair Generation (3) Filtering and Selection (4) Object-centric Preference Optimization with Conditional Preference Loss. Extensive experiments on compositional image generation benchmarks demonstrate that OSPO significantly improves fine-grained alignment in text-to-image generation, surpassing not only prior self-improving methods but also diffusion-based specialized image generation models.

## Introduction

Recent advances in unified Multimodal Large Language Models (MLLMs) (Chen et al. 2025; Wu et al. 2025; Hurst et al. 2024; Deng et al. 2025; Xie et al. 2024; Ge et al. 2023; Sun et al. 2023, 2024; Wang et al. 2024) have expanded their capabilities from text generation to image synthesis. They are generally effective at generating contextually plausible images that capture the overall scene. However, they often fall short in faithfully generating details, such as the spatial relationship or visual attributes of objects specified in the input prompt. Moreover, they frequently hallucinate non-existent objects. These failures are commonly referred to as object hallucination.

To efficiently mitigate this issue without relying on large-scale external datasets or models, several self-improving

methods (Qu et al. 2024; Hong et al. 2025; Mao, Yang, and Shou 2025) have been proposed. However, existing self-improving approaches have not explicitly addressed object-level information for training image generation, preference pair construction, or reward evaluation. As a result, the model is not effectively encouraged to learn which fine-grained object-level distinction it fails to capture or tends to confuse. Consequently, these approaches still suffer from persistent object hallucination problems.<sup>1</sup>

In this work, we propose Object-centric Self-improving Preference Optimization (OSPO), a self-improving framework designed to improve fine-grained object-level text-image alignment. Our preliminary experiments reveal that our baseline model (Chen et al. 2025) struggles with fine-grained object-level text grounding. It often exhibits uncertainty when distinguishing between positive and hard negative texts with slight textual differences and frequently failing to discriminate images with fine-grained object-level differences. Building on this, we introduce a self-improving strategy that self-generates hard preference pairs and performs an object-centric preference optimization using a conditional preference loss to guide the model toward learning fine-grained, object-specific knowledge. Specifically, OSPO consists of four steps: First, we generate initial prompt texts, categorized into four types. Secondly, we generate hard preference pair candidates by generating hard negative images and texts corresponding to the positive samples. Third, we filter out false positives and negatives to reduce noise in training, and select the pairs that the model finds most uncertain. Finally, we perform object-centric preference optimization using the conditional preference loss. We validate the effectiveness of OSPO on three established benchmarks for fine-grained text-to-image generation. Notably, OSPO substantially improves fine-grained alignment, outperforming existing self-improving methods and even surpassing diffusion-based models specifically designed for image generation.

Our main contributions can be summarized as follows:

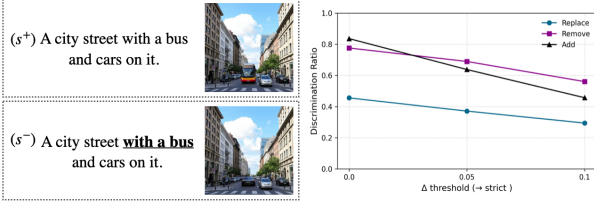
- We propose OSPO, a self-improving framework that precisely focuses on an object-level fine-grained text-to-image generation.
- We introduce an object-centric data construction pipeline including prompt perturbation and densification strat-

<sup>1</sup>A detailed discussion of related work is provided in the Appendix.

\*Corresponding author

### Positive $\leftrightarrow$ Object-level Negative Pair (Type 1)

Identical Input Text / Different Output Images



### Positive $\leftrightarrow$ Object-level Negative Pair (Type 2)

Different Input Texts / Identical Output Image

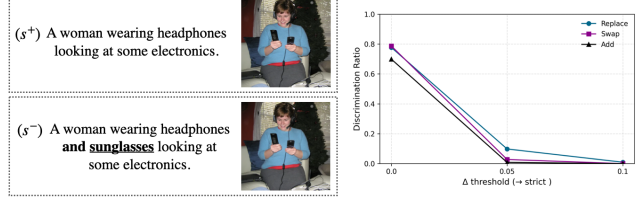


Figure 1: (Left) A pair example, where the text is identical but the images differ in fine-grained details. (Right) A pair example, where the images are identical but the text differs. The graph shows that the discrimination ratio. Replace, Remove, Swap and Add denote perturbation types used to construct the negative samples.

egy and a tailored object-centric optimization where the MLLM generates hard preference pairs and an object-centric conditional preference loss is exploited.

- The proposed OSPO achieves substantial performance improvements on text-to-image benchmarks in terms of the object-level alignment over previous self-improving methods, even outperforming diffusion-based specialized models.

## Preliminary Experiment

In this section, we present a preliminary experiment to motivate our approach that evaluates whether an existing MLLM can confidently discriminate between two images or texts having object-level differences.

## Experiment Setting

**Models and Datasets.** We conduct our experiments using one of the most prominent discrete MLLMs, Janus-Pro-7B (Chen et al. 2025). We construct two types of pairs consisting of a positive  $s^+$  and a negative  $s^-$ : (Type 1) identical text input with different image outputs, and (Type 2) different text inputs with the same image output. The differences are introduced at a fine-grained level, such as replacing a single object region or word. These are constructed using compositional reasoning dataset SugarCrepe (Hsieh et al. 2023) and image editing dataset AnyEdit (Yu et al. 2025). Detailed settings are in the Appendix.

**Metrics.** Based on the average log probability value for the model’s output (image token sequence)  $\mathcal{Z}(x, y) = \frac{1}{|y|} \sum_t \log \pi_\theta(y_t | x, y_{<t})$ , we evaluate discrimination ratio  $\mathcal{D}$  for each pair. It measures the proportion of cases in which the model assigns a higher likelihood to the positive image output than to the negative one, with a margin greater than the threshold  $\Delta$ .

$$\mathcal{D}(s^+, s^-, \Delta) = \frac{1}{N} \sum_{n=1}^N \mathbb{I}[\mathcal{Z}(s_n^+) - \mathcal{Z}(s_n^-) > \Delta], \quad (1)$$

where  $s^+ = (x^+, y^+)$ ,  $s^- \in \{(x^-, y^-), (x^-, y^+)\}$ .  $N$  and  $\mathbb{I}$  denote the number of instances in the evaluation dataset and indicator function.

## Experiment Result

On Type 1 as shown in Figure 1 (Left), the model frequently fails to distinguish the correct image from its negative counterpart (at  $\Delta = 0$ ), even when both are conditioned on the same text input and the negative image contains critical semantic errors at the object level. On Type 2 as shown in Figure 1 (Right), the model demonstrates about 75% correct discrimination at  $\Delta = 0$ . However, the ratio drops sharply with stricter thresholds. This suggests a lack of confidence, as measured by the narrow log-probability gap. This implies that the model is generating output by weakly grounding the input text, despite recognizing the input’s fine-grained difference.

These results motivate us to propose a training framework that leverages fine-grained contrastive pairs generated from the current model and uses a conditional preference loss.

## Method

### Framework Overview

Inspiring by the preliminary experiment, we introduce OSPO: Object-centric Self-improving Preference Optimization framework to enhance fine-grained text-image alignment in MLLMs. The key idea of the framework is to generate fine-grained hard preference pairs  $(t_w, t_\ell)$  and  $(v_w, v_\ell)$  on both the text ( $t$ ) and image ( $v$ ) sides, then train the model using a tailored preference optimization loss. To be specific, the framework consists of four steps: (1) Initial Prompt Generation (2) Hard Preference Pair Generation (3) Filtering and Selection (4) Object-centric Preference Optimization with Conditional Preference Loss. It is noted that as a self-improving frameworks, no external data or models are used during the training. See Figure 2 for the overall framework.

### Step 1: Initial Prompt Generation

Inspired by the T2ICombench++ benchmark (Huang et al. 2025), we organize prompts into four distinct categories: Attribute, Layout, Non-Spatial, and Complex Composition. Leveraging in-context learning (ICL) (Dong et al. 2022) capabilities of MLLMs, we generate initial text prompts for each category ( $x$ ). Specifically, we provide a few-shot

## Preference Data Generation

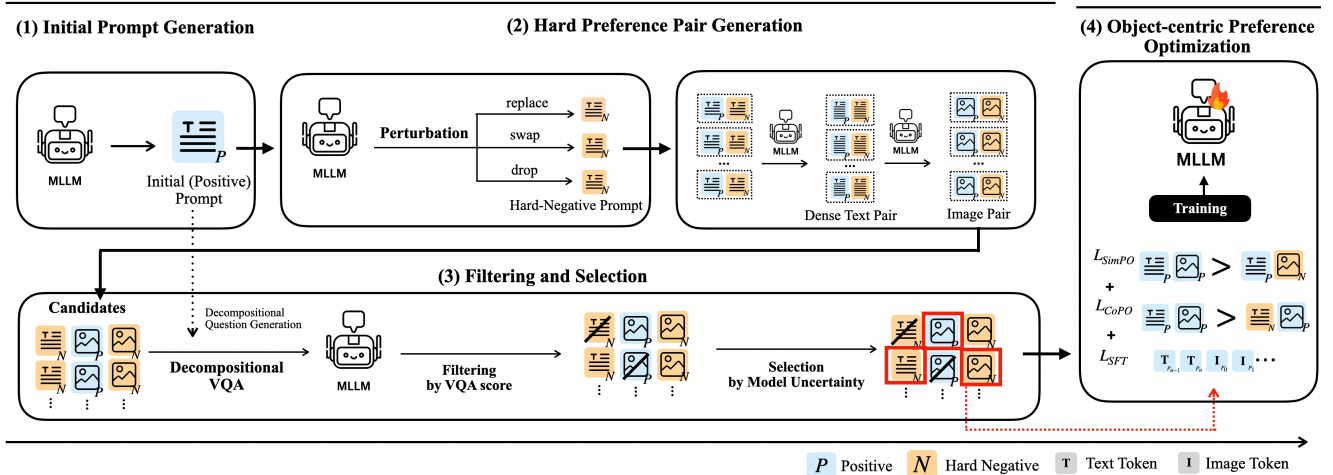


Figure 2: Overview of OSPO framework: (Step 1) MLLM generates initial text prompts referred to as positive prompts. (Step 2) The model perturbs the base prompt using three strategies (Replace, Swap, and Drop) to generate hard negative texts. Each pair of positive and hard negative prompts is densified and used to generate corresponding images, resulting in matched hard negative text–image candidates. (Step 3) The model constructs atomic VQA questions to compare each base sample with its negatives, filtering out false positives or false negatives based on VQA consistency. Then the most confusing pair measured by the log-probability gap is selected. (Step 4) Object-centric Preference Optimization with Conditional Preference Loss, composed of three terms, is applied to fine-tune the MLLM.

demonstration format to guide the model in generating contextually rich and semantically coherent prompts that reflect intricate object interaction and compositional reasoning. Details of the initial input prompts are provided in the Appendix.

### Step 2: Hard Preference Pair Generation

For each text prompt instance  $x$  generated in Step 1, we define a positive sample as either a text or image that preserves the core semantic content of  $x$ . This includes the original prompt itself or an image generated from a densified version of the prompt, both of which maintain the intended meaning. In contrast, a hard negative sample is defined as one that is semantically or visually similar to the positive example, but differs in a fine-grained word or region, thereby potentially confusing the model during alignment. In this step, we generate three types of candidate instances to construct training dataset in the later step: (1) hard negative texts, (2) positive images, and (3) hard negative images. Hereafter, we refer to the original prompt  $x$  as the positive text.

**Hard Negative Text Generation.** Firstly, we generate hard negative texts by applying prompt perturbation to the original prompt  $x$ . Motivated by compositional reasoning benchmarks (Thrush et al. 2022; Hsieh et al. 2023), we adopt three perturbation strategies: Replace, Swap, and Drop. The perturbed data are generated by a current MLLM itself, guided by few-shot examples.

- **replace:** substitute an object or attribute in the prompt with another object or attribute not originally present in the prompt, creating a new combination.

- **swap:** exchange the positions of objects or attributes within the prompt, inducing a different binding than the original prompt.
- **drop:** randomly remove an object or attribute from the prompt, introducing semantic ambiguity.

**Positive and Hard Negative Image Generation.** We start from pairing each positive text prompt with its corresponding three hard negative texts. Since each positive text is paired with three different negative texts, a total of three distinct preference pairs are constructed per positive text. We subsequently generate both positive and hard negative images in a pairwise manner. To generate images that rigorously reflect each corresponding text, we densify positive and negative prompts. Specifically, we densify each positive and negative prompt by adding the same visual context, guiding the model toward more faithful image generation. Densified prompts preserve object-centric contents while adding background or scene descriptions. Through this process, we ultimately generate a total of nine instances for each positive image and its corresponding hard negative images. The prompt templates used in this step are provided in the Appendix.

### Step 3: Filtering and Selection

Among the candidate data generated in the previous step, we identify and select each  $v_w, v_\ell, t_\ell$  for each positive text  $x$ , comprising the winning image, losing image, and corresponding losing text. Winning and Losing denote that preferred and non-preferred in preference learning. Based on insights from preliminary experiment, the samples most confusing to the model due to fine-grained differences that chal-

lenges its current alignment knowledge are selected. In other words, we select the most informative learning pairs. We first perform filtering and selection over image candidates. Subsequently, the selected positive image is used as a visual anchor for the filtering and selection of text candidates. See Algorithm 1 for details.

**Decompositional VQA-based Data Filtering.** The primary objective of data filtering is to eliminate false negative and false positive candidates that may introduce noise into preference training. To this end, we adopt a decompositional VQA approach, which transforms the prompt into a set of atomic semantic units and generates corresponding binary questions. All candidate images including positive images and negative images ( $v$ ) are then evaluated by the score  $s$  answering positive prompt-related questions to assess its semantic alignment with the prompt. This strategy has been widely adopted to improve evaluation reliability (Yu et al. 2024). Finally the filtered positive images  $I'_p$  and filtered negative images  $I'_n$  are constructed as follows:

$$s(v, q_i) = [p(\text{"yes"} | v, q_i) - p(\text{"no"} | v, q_i)], \quad (2)$$

$$I'_p = \{I_p | \forall q_i \in Q(x), s(v, q_i) > \tau\}, \quad (3)$$

$$I'_n = \{I_n | \exists q_i \in Q(x), s(v, q_i) < -\tau\}, \quad (4)$$

, where  $Q(x)$  is a decomposed question set for positive text  $x$  and  $\tau$  is a filtering threshold. We use 0.5 for  $\tau$ .

**Model Uncertainty-based Data Selection.** For each original prompt, we construct a preference pair by selecting the winning and losing elements from the filtered candidates. The original prompt serves as the winning text, and the image with the highest VQA score is selected as the winning image. Given the constructed winning pair  $(t_w, v_w)$ , the losing image and losing text are subsequently identified. Each losing candidate is selected based on the model’s uncertainty in preference judgment, which is the candidate whose log-probability is closest to that of the corresponding winning sample. This minimal log-probability gap indicates that the model is least confident in distinguishing the negative from the positive, making it a hard negative instance that effectively challenges the model’s current alignment boundary. It is important to note that the Selection process relies solely on our own model, which may introduce bias. To assess this, we conducted comparisons with strong external MLLMs. Experimental details and selected pair samples are provided in the Appendix.

#### Step 4: Object-centric Preference Optimization

We introduce a loss function that jointly leverages both hard preference image pairs and hard preference text pairs. Building upon the SimPO (Meng, Xia, and Chen 2024) loss, we propose an OSPO Loss.

$$\mathcal{L}_{\text{SimPO}} = -\mathbb{E}_{(x_w, y_w, y_\ell) \sim \mathcal{D}} \left[ \log \sigma \left( \frac{\beta_1}{|y_w|} \log \pi_\theta(y_w | x_w) - \frac{\beta_1}{|y_\ell|} \log \pi_\theta(y_\ell | x_w) - \gamma_1 \right) \right], \quad (5)$$

---

#### Algorithm 1: Filtering and Selection

---

**Input:** Base Prompt  $x$ , Pos/Neg Candidate Images  $I_p, I_n$ , Neg Candidate Texts  $T_n$ , Model  $\pi_\theta$ , threshold  $\tau$

**Output:**  $v_w, v_\ell, t_w, t_\ell$

```

1:  $t_w \leftarrow x; Q(x) \leftarrow \text{decompose } x \text{ into atomic questions}$ 
2: for all  $v \in I_p \cup I_n, q_i \in Q(x)$  do
3:    $s(v, q_i) \leftarrow p_{\text{yes}} - p_{\text{no}}$ 
4: end for
5:  $I'_p \leftarrow \{v \in I_p | \forall q_i, s(v, q_i) > \tau\}$ 
6:  $I'_n \leftarrow \{v \in I_n | \exists q_i, s(v, q_i) < -\tau\}$ 
7:  $v_w \leftarrow \arg \max_{v \in I'_p} \sum s(v, q_i) / |Q(x)|$ 
8:  $v_\ell \leftarrow \arg \min_{v \in I'_n} |\log p(v_w | x) - \log p(v | x)|$ 
9:  $T'_n \leftarrow \emptyset$ 
10: for all  $t_n \in T_n$  do
11:    $Q(t_n) \leftarrow \text{decompose } t_n$ 
12:   if  $\exists q_i \in Q(t_n)$  s.t.  $s(v_w, q_i) < -\tau$  then
13:      $T'_n \leftarrow T'_n \cup \{t_n\}$ 
14:   end if
15: end for
16:  $t_\ell \leftarrow \arg \min_{t_n} |\log p(v_w | t_w) - \log p(v_w | t_n)|$ 
17: return  $v_w, v_\ell, t_w, t_\ell$ 

```

---

$$\mathcal{L}_{\text{CoPO}} = -\mathbb{E}_{(x_w, x_\ell, y_w) \sim \mathcal{D}} \left[ \log \sigma \left( \frac{\beta_2}{|y_w|} \log \pi_\theta(y_w | x_w) - \frac{\beta_2}{|y_w|} \log \pi_\theta(y_w | x_\ell) - \gamma_2 \right) \right], \quad (6)$$

$$\mathcal{L}_{\text{SFT}} = -\mathbb{E}_{(x_w, y_w) \sim \mathcal{D}} \left[ \frac{1}{|y_w|} \sum_{t=1}^{|y_w|} \log \pi_\theta(y_t | y_{<t}, x_w) \right]$$

$$\mathcal{L}_{\text{OSPO}} = \lambda_1 \mathcal{L}_{\text{SimPO}} + \lambda_2 \mathcal{L}_{\text{CoPO}} + \lambda_3 \mathcal{L}_{\text{SFT}} \quad (7)$$

where  $\pi_\theta$  represents the MLLM and  $x_w, x_\ell, y_w, y_\ell$  represent the input winning text, losing text, output winning image, and losing image from the self-generated preference dataset  $\mathcal{D}$ , respectively. In addition to this,  $\sigma$ ,  $\gamma$ ,  $\beta$ , and  $\lambda$  denote the sigmoid function, target margin, scaling constant for controlling reward difference, and loss weights. The model is optimized through this OSPO loss to capture the fine-grained text-image alignment. It is noted that SILMM (Qu et al. 2024) generates multiple images for a single original prompt, which limits its ability to explicitly capture fine-grained details that confuse the model. In contrast, our method explicitly constructs negative preference pairs and employs the proposed conditional preference loss to enable the model to effectively capture such fine-grained distinctions. Moreover, rather than simply selecting preference pairs from a given dataset, our approach applies a Filtering and Selection process that first filters images misaligned with the prompt and then identifies the negative image that the model finds most confusing. Additionally, the OSPO framework is not limited to a single iteration but can be repeated over multiple iterations, allowing for incremental improvement. Experiments related to this are provided in the Appendix.

| Method                                  | T2I-Compbench++ ↑ |               |               |               |               |               |               |               |  |
|---|-------------------|---------------|---------------|---------------|---------------|---------------|---------------|---------------|--|
|   | Attribute         |               |               | Layout        |               |               | Non-Spatial   | Complex       |  |
|   | Color             | Shape         | Texture       | Spatial-2D    | Spatial-3D    | Numeracy      |               |               |  |
| <b>Diffusion Models</b>                 |                   |               |               |               |               |               |               |               |  |
| SD-XL                                   | 0.6369            | 0.5408        | 0.5637        | 0.2032        | -             | -             | 0.3110        | 0.4091        |  |
| DALL-E 3                                | 0.7785            | 0.6205        | 0.7036        | 0.2865        | -             | -             | 0.3003        | 0.3773        |  |
| FLUX.1                                  | 0.7407            | 0.5718        | 0.6922        | 0.2863        | -             | -             | 0.3127        | 0.3703        |  |
| <b>Multimodal Large Language Models</b> |                   |               |               |               |               |               |               |               |  |
| Show-o                                  | 0.5600            | 0.4100        | 0.4600        | 0.2000        | -             | -             | 0.3000        | 0.2900        |  |
| Janus                                   | 0.7453            | 0.4672        | 0.6142        | 0.1571        | 0.3212        | 0.5230        | 0.3110        | 0.3483        |  |
| Emu3                                    | 0.7544            | 0.5706        | 0.7164        | -             | -             | -             | -             | -             |  |
| Unitok                                  | 0.7745            | 0.5195        | 0.6431        | 0.2668        | <b>0.4088</b> | <u>0.5675</u> | 0.3131        | 0.3617        |  |
| Janus-Pro-7B                            | 0.5215            | 0.3272        | 0.4050        | 0.1654        | 0.2679        | 0.4431        | 0.3109        | 0.3868        |  |
| + SILMM                                 | 0.7394            | 0.4325        | 0.5796        | 0.2105        | 0.3572        | 0.5073        | 0.3113        | 0.3725        |  |
| + DSR                                   | 0.7824            | 0.5786        | 0.7292        | 0.2524        | -             | -             | <u>0.3141</u> | 0.3858        |  |
| + T2I-R1                                | 0.8130            | 0.5852        | 0.7243        | <u>0.3378</u> | -             | -             | 0.3090        | <u>0.3993</u> |  |
| <b>+ OSPO (ours)</b>                    | <b>0.8438</b>     | <b>0.6268</b> | <b>0.7782</b> | <b>0.3522</b> | <u>0.3839</u> | <b>0.5889</b> | <b>0.3169</b> | <b>0.4184</b> |  |

Table 1: Comparison on T2I-CompBench++ (Huang et al. 2025). ↑ indicates higher is better. Bold highlights the best scores among Multimodal LLMs. Underline indicates the second-highest scores among Multimodal LLMs.

| Method                                  | DPGBench ↑   |              |              |              |              |              | GenEval ↑   |             |             |             |             |                   |             |
|---|--------------|--------------|--------------|--------------|--------------|--------------|-------------|-------------|-------------|-------------|-------------|-------------------|-------------|
|   | Attribute    | Relation     | Entity       | Other        | Global       | Total        | Single      | Two         | Count       | Colors      | Position    | Color Attribution | Total       |
| <b>Diffusion Models</b>                 |              |              |              |              |              |              |             |             |             |             |             |                   |             |
| SD-XL                                   | 82.43        | 80.91        | 86.76        | 80.41        | 83.27        | 74.65        | 0.98        | 0.74        | 0.39        | 0.85        | 0.15        | 0.15              | 0.55        |
| DALL-E 3                                | 89.61        | 88.39        | 90.58        | 89.83        | 90.97        | 83.50        | 0.96        | 0.87        | 0.47        | 0.83        | 0.43        | 0.43              | 0.67        |
| SD3                                     | -            | -            | -            | -            | -            | -            | 0.99        | 0.94        | 0.72        | 0.89        | 0.33        | 0.60              | 0.74        |
| <b>Multimodal Large Language Models</b> |              |              |              |              |              |              |             |             |             |             |             |                   |             |
| Show-o                                  | -            | -            | -            | -            | -            | -            | 0.98        | 0.80        | <u>0.66</u> | 0.84        | 0.31        | 0.50              | 0.68        |
| Janus                                   | 85.96        | 88.15        | 83.06        | 82.76        | 77.04        | 75.33        | 0.97        | 0.68        | 0.30        | 0.84        | 0.46        | 0.42              | 0.61        |
| Emu3                                    | 86.33        | 90.61        | 87.17        | <b>89.75</b> | 87.54        | 81.60        | 0.98        | 0.69        | 0.33        | 0.78        | 0.15        | 0.16              | 0.52        |
| Unitok                                  | 88.37        | 91.39        | 88.13        | 87.54        | 83.98        | 81.87        | 0.99        | 0.75        | 0.39        | 0.80        | 0.21        | 0.41              | 0.59        |
| Jauns-Pro-7B                            | 86.11        | <b>92.72</b> | 88.30        | <u>88.85</u> | 82.62        | 83.81        | 0.98        | 0.87        | 0.57        | 0.89        | 0.78        | 0.67              | 0.80        |
| + SILMM                                 | 89.47        | 91.26        | <b>90.33</b> | 88.37        | <b>91.46</b> | 84.56        | 0.98        | 0.87        | 0.58        | 0.90        | 0.77        | <u>0.71</u>       | 0.80        |
| + DSR                                   | -            | -            | -            | -            | -            | -            | <u>0.99</u> | <u>0.89</u> | <b>0.70</b> | <b>0.92</b> | <b>0.82</b> | <u>0.71</u>       | <b>0.84</b> |
| + T2I-R1                                | <u>89.92</u> | 91.82        | 89.78        | 88.67        | 88.82        | 85.09        | <b>1.00</b> | <b>0.91</b> | 0.52        | 0.90        | 0.77        | 0.65              | 0.79        |
| <b>+ OSPO (ours)</b>                    | <b>90.16</b> | 92.34        | <u>90.22</u> | 84.22        | <u>90.36</u> | <b>85.34</b> | 0.98        | <u>0.89</u> | 0.60        | <u>0.91</u> | 0.79        | <b>0.74</b>       | <u>0.82</u> |

Table 2: Comparison on DPGBench (Hu et al. 2024) and GenEval (Ghosh, Hajishirzi, and Schmidt 2023). ↑ indicates higher is better. Bold highlights the best scores among Multimodal LLMs. Underline indicates the second-highest scores among Multimodal LLMs.

## Experiments

### Experiment Setting

**Models.** We conducted experiments using Janus-Pro-7B (Chen et al. 2025) as the primary backbone model. Additionally, we extended our experiments to include models based on the Janus-1.3B (Wu et al. 2025) and Unitok-MLLM-7B(Ma et al. 2025a) backbones for comparative analysis.

**Baselines.** To evaluate the effectiveness of the proposed self-improving framework, we compare it with other self-improving framework for text-to-image generation. For example, we consider SILMM (Qu et al. 2024), DSR (Hong et al. 2025) and UniRL (Mao, Yang, and Shou 2025) as the baseline frameworks<sup>2</sup> that construct preference pairs by gen-

erating images and rewarding them without reliance on any external supervision. Also, we consider T2I-R1 (Jiang et al. 2025), which is not a self-improving method, but performs preference optimization for text-to-image generation with self-constructed data using external models. For fair comparison, we reproduced several methods on top of the same backbone model.

**Benchmarks.** We evaluated models’ text-to-image generation capabilities on three established benchmarks: **T2I-CompBench++** (Huang et al. 2025), **DPGBench** (Hu et al. 2024), and **GenEval** (Ghosh, Hajishirzi, and Schmidt 2023). Each evaluation was conducted following the standard configurations and protocols. For a detailed explanation of each benchmark, please refer to the Appendix.

**Training Prompts.** We generated a total of 19,000 text prompt datasets evenly distributed across four different cat-

<sup>2</sup>While DSR and UniRL address both image generation and understanding, we constrain our focus to image generation.

| Method                                 | T2ICompBench++      |             |             |             | DPGBench              | GenEval             |
|--|---------------------|-------------|-------------|-------------|-----------------------|---------------------|
|  | A                   | L           | NS          | C           | Overall               | Overall             |
| Unitok-MLLM-7B<br>+ OSPO (ours)        | 0.65<br><b>0.68</b> | <b>0.41</b> | 0.31        | 0.36        | 81.87<br><b>83.34</b> | 0.59<br><b>0.62</b> |
| Janus-1.3B<br>+ UniRL<br>+ OSPO (ours) | 0.62                | 0.34        | 0.31        | 0.35        | 75.33                 | 0.59                |
|  | -                   | -           | -           | -           | -                     | 0.65                |
|  | <b>0.68</b>         | <b>0.38</b> | <b>0.32</b> | <b>0.37</b> | <b>81.94</b>          | <b>0.68</b>         |

Table 3: Performance comparison across model variants with different architectures and scales on T2ICompBench++, DPGBench, and GenEval. A, L, NS, and C denote the Attribute, Layout, Non-Spatial, and Complex categories, respectively.

egories (Attribute, Layout, Non-spatial, Complex Composition).

**Implementation Details.** All experiments were conducted using four NVIDIA A100 GPUs. More details are provided in the Appendix.

## Main Results

As presented in Table 1, OSPO-trained model outperforms all baseline methods on the T2I-CompBench++ benchmark. Notably, the substantial improvements are observed in the Attribute category, while the Non-spatial or Complex category shows relatively smaller improvements. This disparity is attributed to the difference of metric measuring each category and the nature of CLIP-T score (Radford et al. 2021; Hessel et al. 2021) measuring Non-spatial and Complex, which is known to exhibit lower sensitivity in scoring range. In this context, comparison with other methods or models demonstrates that our model performs comparably well in the those categories. The model demonstrates consistent improvements on other benchmarks as well. On DPGBench, our model achieves the highest overall score. This demonstrates strong generalization even to out-of-distribution, harder long-form prompts that were not seen during training. Representative examples generated by the OSPO-trained model are shown in Figure 3, with additional samples provided in the Appendix.

Our model also achieves the second-best overall score on the GenEval benchmark. While T2I-CompBench++ emphasizes compositional reasoning under complex prompts that challenge the model’s ability to go beyond its language priors, in contrast, GenEval places greater weight on literal correctness. It is important to recognize that some baseline models are trained with additional supervision. For example, DSR incorporates vision-language understanding tasks during training, and T2I-R1 leverages external datasets along with multiple reward models. These elements likely contribute to their strong performance on GenEval, as they offer more explicit supervision and broader visual-textual coverage. In comparison, our model does not rely on such external resources. Nonetheless, it achieves competitive results across categories and outperforms the fully self-improving baseline SILMM. This highlights the robustness of our approach, even under more restricted environments. Additionally, we applied a test-time scaling approach that uses the

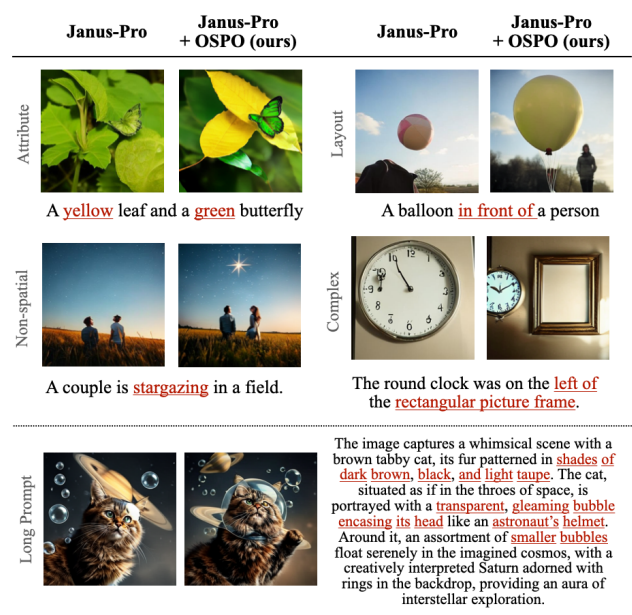


Figure 3: Qualitative results of Janus-Pro + OSPO from T2I-CompBench++ and DPGBench.

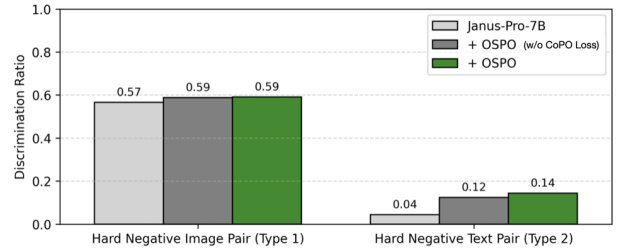


Figure 4: Discrimination Ratio (at  $\Delta = 0.05$ ) in Eq (1) comparison between Janus-Pro, Janus-Pro + OSPO (w/o  $L_{CoPO}$ ) and Janus-Pro + OSPO.

VQA strategy in OSPO to evaluate and select from multiple sampled images, leading to further performance improvements on the benchmark. Details of these experiments are provided in the Appendix.

To investigate the model-agnostic applicability of our framework, we conduct additional experiments using two alternative MLLMs: UniTok-MLLM (Ma et al. 2025a) with a different architecture and Janus (Wu et al. 2025) with lower capacity. Both models exhibit notably weaker image understanding and reasoning capabilities compared to Janus-Pro, which are critical for our data generation pipeline. As shown in Table 3 and 4, applying the OSPO framework consistently improves performances across both models. These results validate the generalizability and effectiveness of our framework across a diverse set of MLLMs.

## Ablation Studies and Analyses

**OSPO improves fine-grained discrimination with confidence.** To evaluate the effectiveness of OSPO in fine-

| Method   | T2ICompBench++ |             |             |             | DPGBench     | GenEval     |
|--|----------------|-------------|-------------|-------------|--------------|-------------|
|  | A              | L           | NS          | C           | Overall      | Overall     |
| OSPO   | 0.75           | <b>0.44</b> | <b>0.32</b> | <b>0.42</b> | 85.34        | <b>0.82</b> |
| w/o $\mathcal{L}_{CoPO}$                       | 0.74           | 0.43        | <b>0.32</b> | 0.41        | 84.94        | 0.81        |
| w/o $\mathcal{L}_{SFT}$                        | 0.77           | 0.43        | <b>0.32</b> | 0.41        | 85.65        | 0.81        |
| w/o $\mathcal{L}_{CoPO}$ , $\mathcal{L}_{SFT}$ | <b>0.78</b>    | 0.39        | 0.31        | 0.40        | <b>86.10</b> | 0.77        |

Table 4: Performance comparison across loss ablations on T2ICompBench++, DPGBench, and GenEval.

grained compositional generation, we measure the discrimination ratio as defined in Eq.(1) by presenting the model with hard preference pairs. As shown in Figure 4, OSPO improves the discrimination ratio across both image-based and text-based cases. In particular, we observe substantial gains on text pairs, where original models typically struggle. These results suggest that OSPO enhances the model’s sensitivity to subtle compositional differences, improving its ability to align with fine-grained semantic cues during generation.

**Loss composition mediates the trade-off between expressiveness and precision in compositional generation.** An ablation study is conducted to assess the role of each loss component in our object-centric optimization framework. Using only the SimPO loss increases visual expressiveness but leads to object over-generation that degrades image coherence. This behavior increases recall by generating a wider range of objects, which can improve scores on VQA-based benchmarks that reward partial correctness. However, it reduces precision and harms performance on detector-based benchmarks that require accurate object count and penalize over-generation. Adding either the supervised loss or the text-conditional preference loss mitigates this issue by preventing the model from overfitting too aggressively to the SimPO objective and enforcing stronger textual grounding. The best results are achieved when both are combined, balancing expressive alignment with structural accuracy.

**Filtering and selection during data construction enhance the quality of preference supervision.** To evaluate the effectiveness of filtering and selection in OSPO, we perform an ablation on the training dataset construction. Specifically, we compare models trained on differently curated preference triplets. One variant uses no filtering or selection and trains on all 19,000 randomly sampled triplets. Another applies filtering based on VQA score but selects triplets randomly from the filtered set. As shown in Table 5, applying both filtering and selection yields the best performance across all benchmarks. Filtering alone provides marginal improvements, while selection plays a more critical role in aligning preference pairs with fine-grained semantic distinctions, particularly in GenEval and DPGBench.

**Prompt densification improves training image quality and strengthens compositional alignment.** To improve the semantic fidelity of generated training images, we incorporate a prompt densification step during candidate image generation. To examine its impact, we compare the full OSPO framework with a variant trained without the densi-

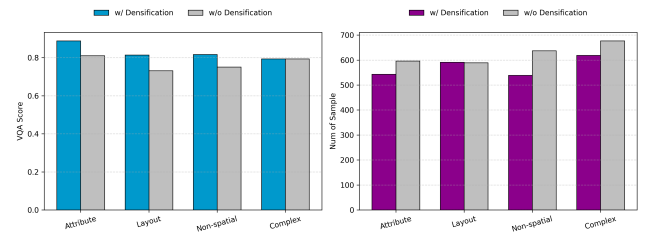


Figure 5: Comparison of VQA scores and the number of samples where the model correctly distinguishes the winning and losing images.

| Filtering | Selection | T2ICompBench++ |             |             |             | DPGBench     | GenEval     |
|-----------|-----------|----------------|-------------|-------------|-------------|--------------|-------------|
|           |           | A              | L           | NS          | C           | Overall      | Overall     |
| ✓         | ✓         | <b>0.75</b>    | <b>0.44</b> | <b>0.32</b> | <b>0.42</b> | <b>85.34</b> | <b>0.82</b> |
| ✓         | ✗         | 0.75           | 0.43        | 0.32        | 0.41        | 84.84        | 0.81        |
| ✗         | ✗         | 0.73           | 0.43        | 0.32        | 0.40        | 84.84        | 0.80        |

Table 5: Performance comparison across filtering and selection ablations on T2ICompBench++, DPGBench, and GenEval. ✓: applied, ✗: not applied.

| Method            | T2ICompBench++ |             |             |             | DPGBench     | GenEval     |
|-------------------|----------------|-------------|-------------|-------------|--------------|-------------|
|                   | A              | L           | NS          | C           | Overall      | Overall     |
| w/ Densification  | <b>0.75</b>    | <b>0.44</b> | <b>0.32</b> | <b>0.42</b> | <b>85.34</b> | <b>0.82</b> |
| w/o Densification | 0.61           | 0.34        | 0.31        | 0.39        | 85.16        | 0.81        |

Table 6: Performance comparison on Densification.

fication step, where candidate images are generated directly from the original prompts without modification. As shown in Figure 5 and Table 6, removing densification leads to a clear performance drop across benchmarks. Also, densification makes improvement in image fidelity and positive and negative image pair more difficult to distinguish. These results indicate that both the informativeness of training image pairs and the visual quality of the selected positive image influence the effectiveness of the framework.

## Conclusion

We present a **Object-centric Self-improving Preference Optimization (**OSPO**)** framework for text-to-image generation in MLLMs. Our framework leverages the unified multimodal processing capabilities of MLLMs, enhancing their fine-grained text-image alignment performances without the need for external datasets or additional models. By generating hard preference pairs and applying an object-centric preference optimization with a conditional preference loss, the model effectively self-improves its ability to capture fine-grained object-level details. Experiments on compositional image generation benchmarks show that OSPO greatly enhances fine-grained alignment in text-to-image generation, outperforming both prior self-improving methods and diffusion-based models.

## Acknowledgements

This work was partly supported by Institute of Information & communications Technology Planning & Evaluation (IITP) grant funded by the Korea government(MSIT) (No. RS-2019-II190079, Artificial Intelligence Graduate School Program(Korea University), 15%), the Institute of Information & Communications Technology Planning & Evaluation(IITP)-ITRC(Information Technology Research Center) grant funded by the Korea government(MSIT)(IITP-2025-RS-2024-00436857, 35%), and the National Research Foundation of Korea(NRF) grant funded by the Korea government(MSIT) (No. RS-2024-00353007, 50%).

## References

- Bai, S.; Chen, K.; Liu, X.; Wang, J.; Ge, W.; Song, S.; Dang, K.; Wang, P.; Wang, S.; Tang, J.; et al. 2025. Qwen2. 5-vl technical report. *arXiv preprint arXiv:2502.13923*.
- Chen, X.; Wu, Z.; Liu, X.; Pan, Z.; Liu, W.; Xie, Z.; Yu, X.; and Ruan, C. 2025. Janus-pro: Unified multimodal understanding and generation with data and model scaling. *arXiv preprint arXiv:2501.17811*.
- Deng, C.; Zhu, D.; Li, K.; Gou, C.; Li, F.; Wang, Z.; Zhong, S.; Yu, W.; Nie, X.; Song, Z.; et al. 2025. Emerging properties in unified multimodal pretraining. *arXiv preprint arXiv:2505.14683*.
- Dong, Q.; Li, L.; Dai, D.; Zheng, C.; Ma, J.; Li, R.; Xia, H.; Xu, J.; Wu, Z.; Liu, T.; et al. 2022. A survey on in-context learning. *arXiv preprint arXiv:2301.00234*.
- Esser, P.; Rombach, R.; and Ommer, B. 2021. Taming transformers for high-resolution image synthesis. In *Proceedings of the IEEE/CVF conference on computer vision and pattern recognition*, 12873–12883.
- Ge, Y.; Zhao, S.; Zeng, Z.; Ge, Y.; Li, C.; Wang, X.; and Shan, Y. 2023. Making llama see and draw with seed tokenizer. *arXiv preprint arXiv:2310.01218*.
- Ghosh, D.; Hajishirzi, H.; and Schmidt, L. 2023. Geneval: An object-focused framework for evaluating text-to-image alignment. *Advances in Neural Information Processing Systems*, 36: 52132–52152.
- Guo, D.; Yang, D.; Zhang, H.; Song, J.; Zhang, R.; Xu, R.; Zhu, Q.; Ma, S.; Wang, P.; Bi, X.; et al. 2025. Deepseek-r1: Incentivizing reasoning capability in llms via reinforcement learning. *arXiv preprint arXiv:2501.12948*.
- Hessel, J.; Holtzman, A.; Forbes, M.; Bras, R. L.; and Choi, Y. 2021. Clipscore: A reference-free evaluation metric for image captioning. *arXiv preprint arXiv:2104.08718*.
- Hong, J.; Zhang, Y.; Wang, G.; Liu, Y.; Wen, J.-R.; and Yan, R. 2025. Reinforcing Multimodal Understanding and Generation with Dual Self-rewards. *arXiv preprint arXiv:2506.07963*.
- Hsieh, C.-Y.; Zhang, J.; Ma, Z.; Kembhavi, A.; and Krishna, R. 2023. Sugarcrape: Fixing hackable benchmarks for vision-language compositionality. *Advances in neural information processing systems*, 36: 31096–31116.
- Hu, X.; Wang, R.; Fang, Y.; Fu, B.; Cheng, P.; and Yu, G. 2024. Ella: Equip diffusion models with llm for enhanced semantic alignment. *arXiv preprint arXiv:2403.05135*.
- Huang, K.; Duan, C.; Sun, K.; Xie, E.; Li, Z.; and Liu, X. 2025. T2I-CompBench++: An Enhanced and Comprehensive Benchmark for Compositional Text-to-Image Generation. *IEEE Transactions on Pattern Analysis and Machine Intelligence*.
- Hurst, A.; Lerer, A.; Goucher, A. P.; Perelman, A.; Ramesh, A.; Clark, A.; Ostrow, A.; Welihinda, A.; Hayes, A.; Radford, A.; et al. 2024. Gpt-4o system card. *arXiv preprint arXiv:2410.21276*.
- Jiang, D.; Guo, Z.; Zhang, R.; Zong, Z.; Li, H.; Zhuo, L.; Yan, S.; Heng, P.-A.; and Li, H. 2025. T2i-r1: Reinforcing image generation with collaborative semantic-level and token-level cot. *arXiv preprint arXiv:2505.00703*.
- Ma, C.; Jiang, Y.; Wu, J.; Yang, J.; Yu, X.; Yuan, Z.; Peng, B.; and Qi, X. 2025a. Unitok: A unified tokenizer for visual generation and understanding. *arXiv preprint arXiv:2502.20321*.
- Ma, Y.; Liu, X.; Chen, X.; Liu, W.; Wu, C.; Wu, Z.; Pan, Z.; Xie, Z.; Zhang, H.; Yu, X.; et al. 2025b. Janusflow: Harmonizing autoregression and rectified flow for unified multimodal understanding and generation. In *Proceedings of the Computer Vision and Pattern Recognition Conference*, 7739–7751.
- Mao, W.; Yang, Z.; and Shou, M. Z. 2025. UniRL: Self-Improving Unified Multimodal Models via Supervised and Reinforcement Learning. *arXiv preprint arXiv:2505.23380*.
- Meng, Y.; Xia, M.; and Chen, D. 2024. Simpo: Simple preference optimization with a reference-free reward. *Advances in Neural Information Processing Systems*, 37: 124198–124235.
- Qu, L.; Li, H.; Wang, W.; Liu, X.; Li, J.; Nie, L.; and Chua, T.-S. 2024. SILMM: Self-Improving Large Multimodal Models for Compositional Text-to-Image Generation. *arXiv preprint arXiv:2412.05818*.
- Radford, A.; Kim, J. W.; Hallacy, C.; Ramesh, A.; Goh, G.; Agarwal, S.; Sastry, G.; Askell, A.; Mishkin, P.; Clark, J.; et al. 2021. Learning transferable visual models from natural language supervision. In *International conference on machine learning*, 8748–8763. PmLR.
- Rafailov, R.; Sharma, A.; Mitchell, E.; Manning, C. D.; Ermon, S.; and Finn, C. 2023. Direct preference optimization: Your language model is secretly a reward model. *Advances in Neural Information Processing Systems*, 36: 53728–53741.
- Sun, Q.; Cui, Y.; Zhang, X.; Zhang, F.; Yu, Q.; Wang, Y.; Rao, Y.; Liu, J.; Huang, T.; and Wang, X. 2024. Generative multimodal models are in-context learners. In *Proceedings of the IEEE/CVF Conference on Computer Vision and Pattern Recognition*, 14398–14409.
- Sun, Q.; Yu, Q.; Cui, Y.; Zhang, F.; Zhang, X.; Wang, Y.; Gao, H.; Liu, J.; Huang, T.; and Wang, X. 2023. Emu: Generative pretraining in multimodality. *arXiv preprint arXiv:2307.05222*.
- Thrush, T.; Jiang, R.; Bartolo, M.; Singh, A.; Williams, A.; Kiela, D.; and Ross, C. 2022. Winoground: Probing vision and language models for visio-linguistic compositionality. In *Proceedings of the IEEE/CVF Conference on Computer Vision and Pattern Recognition*, 5238–5248.

Van Den Oord, A.; Vinyals, O.; et al. 2017. Neural discrete representation learning. *Advances in neural information processing systems*, 30.

Wang, X.; Zhang, X.; Luo, Z.; Sun, Q.; Cui, Y.; Wang, J.; Zhang, F.; Wang, Y.; Li, Z.; Yu, Q.; et al. 2024. Emu3: Next-token prediction is all you need. *arXiv preprint arXiv:2409.18869*.

Wu, C.; Chen, X.; Wu, Z.; Ma, Y.; Liu, X.; Pan, Z.; Liu, W.; Xie, Z.; Yu, X.; Ruan, C.; et al. 2025. Janus: Decoupling visual encoding for unified multimodal understanding and generation. In *Proceedings of the Computer Vision and Pattern Recognition Conference*, 12966–12977.

Wu, Y.; Zhang, Z.; Chen, J.; Tang, H.; Li, D.; Fang, Y.; Zhu, L.; Xie, E.; Yin, H.; Yi, L.; et al. 2024. Vila-u: a unified foundation model integrating visual understanding and generation. *arXiv preprint arXiv:2409.04429*.

Xie, J.; Mao, W.; Bai, Z.; Zhang, D. J.; Wang, W.; Lin, K. Q.; Gu, Y.; Chen, Z.; Yang, Z.; and Shou, M. Z. 2024. Show-o: One single transformer to unify multimodal understanding and generation. *arXiv preprint arXiv:2408.12528*.

Yu, Q.; Chow, W.; Yue, Z.; Pan, K.; Wu, Y.; Wan, X.; Li, J.; Tang, S.; Zhang, H.; and Zhuang, Y. 2025. Anyedit: Mastering unified high-quality image editing for any idea. In *Proceedings of the Computer Vision and Pattern Recognition Conference*, 26125–26135.

Yu, T.; Zhang, H.; Yao, Y.; Dang, Y.; Chen, D.; Lu, X.; Cui, G.; He, T.; Liu, Z.; Chua, T.-S.; et al. 2024. Rlaif-v: Aligning mllms through open-source ai feedback for super gpt-4v trustworthiness. *arXiv preprint arXiv:2405.17220*.

## Appendix

The following sections provide a thorough examination of our experimental results. Specifically, they include detailed descriptions of related work, evaluation benchmarks, implementation details, additional analyses, and qualitative image examples.

### A. Related Works

**A.1. Multimodal Large Language Models (MLLMs)** While early Multimodal Large Language Models (MLLMs), especially for large vision-language models, primarily extended pretrained LLMs to support visual understanding by incorporating vision encoders, recent advances have moved toward unified LLMs that can both understand and generate visual content. This unification enables a single model to handle diverse tasks, ranging from image understanding to image generation, under a shared autoregressive framework. Representative works in this line of research include models such as SEED-LLaMA (Ge et al. 2023), VILA-U (Wu et al. 2024), Show-o (Xie et al. 2024), Emu3 (Wang et al. 2024), Janus series (Wu et al. 2025; Ma et al. 2025b; Chen et al. 2025), and UniTok (Ma et al. 2025a) that leverage Vector Quantization (VQ) (Van Den Oord, Vinyals et al. 2017; Esser, Rombach, and Ommer 2021) based tokenizers to discretize images into tokens, thereby allowing both vision and language to be modeled uniformly through next-token prediction. In this work, we also focus on these autoregressive, discrete unified MLLMs particularly for text-to-image generation.

**A.2. Self-Improving Text-to-Image Generation in MLLMs** Recent advances in unified MLLMs have opened the door to self-improving approaches for text-to-image generation (Qu et al. 2024; Hong et al. 2025; Mao, Yang, and Shou 2025). Most of these methods adopt preference-based learning frameworks such as DPO (Rafailov et al. 2023), SimPO (Meng, Xia, and Chen 2024) and GRPO (Guo et al. 2025), leveraging self-generated preference datasets. Without relying on external data or reward models, they synthesize image samples and derive rewards in a self-supervised manner. However, these methods rely on simple *Best-of-N* sampling strategy during data generation, which fails to provide explicit object-level contrast between images. Moreover, their reward evaluation or selection strategies typically operates at a global level without accounting for fine-grained object-level distinctions. For example, selection is often based on the average log-probability over the entire sequence of image tokens. These limits the model’s ability to internalize object-level distinctions and constrains the overall improvement in object fidelity. In contrast, our proposed OSPO framework explicitly incorporates object-level supervision throughout both the data generation and reward evaluation processes, enabling more targeted supervision and facilitating the learning of fine-grained object semantics.

## B. Evaluation Benchmarks

### B.1. T2ICompbench++

T2ICompBench++ (Huang et al. 2025) evaluates compositional image generation performances using 2,400 text

prompts, organized into four primary categories: Attribute, Layout, Non-spatial, and Complex Composition. It further comprises eight sub-categories—color, shape, texture, 2D spatial, 3D spatial, numeracy, non-spatial, and complex—each assessed with distinct evaluation criteria. Each category is evaluated using a distinct metric: the Attribute category is assessed based on VQA scores from a Vision-Language Model (VLM); the Layout category relies on detector-based spatial accuracy; the Non-spatial category uses CLIP-T similarity scores; and the Complex category aggregates the above metrics to provide a holistic evaluation. Unlike other benchmarks, T2I-CompBench++ includes image generation tasks that challenge the model’s common-sense understanding by presenting unfamiliar and compositional prompts.

### B.2. DPGBench

DPGBench (Hu et al. 2024) evaluates compositional image generation performances with 1,065 long and semantically rich text prompts, which have an average token length of 83.91. This benchmark is designed to measure models’ ability to align with complex semantic structures in extended narratives.

### B.3. GenEval

GenEval (Ghosh, Hajishirzi, and Schmidt 2023) evaluates object-focused image generation performances with 550 text prompts, structured into six primary categories: Single Object, Two Objects, Counting, Colors, Position, and Attribute Binding. The text prompt format is markedly different from T2I-CompBench++.

## C. Implementation Details

### C.1. Preliminary Experiment

We construct two types of object-level preference pairs to evaluate fine-grained text-image alignment. In both types, positive and negative denote whether the output image accurately reflects the input prompt without object-level hallucination. We detail the construction process below.

- **Type 1: Same Text Input, Different Image Outputs** We sample 1,000 instances from the AnyEdit (Yu et al. 2025) validation set and group them into Replace, Remove, and Add based on the editing type. Each instance consists of an edit instruction, a before-edit image, an after-edit image, a caption for the before image, and a caption for the after image. Using these instances, we construct a positive-negative sequence pair. Depending on the category, either the before- or after-editing image is designated as the positive, with the other as the negative. The caption corresponding to the positive image is used as the input prompt. Using the prompt and the positive-negative image pair, we construct two text-image sequences capturing fine-grained object-level differences.
- **Type 2: Different Text Inputs, Same Image Output** We sample 1,000 instances from the SugarCrepe (Hsieh et al. 2023) validation set. Each original instance consists of an image and a triplet of captions: two semantically equivalent but lexically different positive captions, and one

| Configuration             | Janus-Pro-7B                                     | UniTok-MLLM-7B                                   | Janus-1.3B                                       |
|---------------------------|--|--|--|
| LoRA Rank                 | 32   | 32   | 32   |
| LoRA Alpha                | 64   | 64   | 64   |
| Optimizer                 | AdamW  | AdamW  | AdamW  |
| Optimizer Hyperparameters | $\beta_1: 0.9, \beta_2: 0.95, \epsilon: 1e-8$    | $\beta_1: 0.9, \beta_2: 0.95, \epsilon: 1e-8$    | $\beta_1: 0.9, \beta_2: 0.95, \epsilon: 1e-8$    |
| Gradient Clipping         | 1.0  | 1.0  | 1.0  |
| Weight Decay              | 0.0  | 0.0  | 0.0  |
| Learning Rate             | 1e-5   | 6e-6   | 1e-5   |
| Learning Rate Scheduler   | Constant   | Constant   | Constant   |
| Total Training Steps      | 330  | 300  | 500  |
| Accumulation Steps        | 4  | 4  | 1  |
| Total Batch Size          | 128  | 128  | 64   |
| Beta Weight               | $\beta_1: 3, \beta_2: 5$                         | $\beta_1: 3, \beta_2: 5$                         | $\beta_1: 5, \beta_2: 5$                         |
| Gamma Weight              | $\gamma_1: 0.5, \gamma_2: 0.5$                   | $\gamma_1: 0.5, \gamma_2: 0.5$                   | $\gamma_1: 0.5, \gamma_2: 0.5$                   |
| Loss Weight               | $\lambda_1: 0.8, \lambda_2: 1.5, \lambda_3: 0.5$ | $\lambda_1: 0.8, \lambda_2: 1.5, \lambda_3: 0.5$ | $\lambda_1: 1.0, \lambda_2: 1.5, \lambda_3: 0.5$ |
| GPU                       | 4 × A100 80GB                                    | 4 × A100 80GB                                    | 4 × A100 80GB                                    |
| Mixed Precision           | bf16   | bf16   | bf16   |
| Flash Attention Version   | 2  | 2  | 2  |

Table 7: Comparison of training settings for Janus-Pro-7B, UniTok-MLLM-7B, and Janus-1.3B.

| Method           | T2I-ComPbench++ ↑ |               |               |               |               |               |               |               | DPG Bench    | GenEval     |  |  |
|------------------|-------------------|---------------|---------------|---------------|---------------|---------------|---------------|---------------|--------------|-------------|--|--|
|                  | Attribute         |               |               | Layout        |               |               | Non-Spatial   | Complex       |              |             |  |  |
|                  | Color             | Shape         | Texture       | Spatial-2D    | Spatial-3D    | Numeracy      |               |               |              |             |  |  |
| Janus-Pro-7B     | 0.5215            | 0.3272        | 0.405         | 0.1654        | 0.2679        | 0.4431        | 0.3109        | 0.3868        | 83.81        | 0.80        |  |  |
| + OSPO (Iter. 1) | 0.8438            | 0.6268        | 0.7782        | <b>0.3522</b> | 0.3839        | <b>0.5889</b> | 0.3169        | <b>0.4184</b> | 85.34        | <b>0.82</b> |  |  |
| + OSPO (Iter. 2) | <b>0.8600</b>     | <b>0.6343</b> | <b>0.7786</b> | 0.3510        | <b>0.3945</b> | 0.5749        | <b>0.3175</b> | 0.4112        | <b>85.53</b> | <b>0.82</b> |  |  |

Table 8: Performance improvement of Janus-Pro-7B with OSPO over two iterations.

hard negative caption. The hard negative captions are deliberately constructed to contain fine-grained factual errors and are categorized into three types based on the nature of the error: Replace, Swap, and Add. For each image, we construct a contrastive prompt pair by selecting one positive caption and pairing it with the corresponding hard negative caption. Since the SugarCrepe dataset is designed to assess compositional understanding by introducing precise mismatches between the image and the caption, we utilize this property to form challenging evaluation pairs. The same image is used as output, and each prompt serves as input. This forms two text-to-image sequences differing only in textual composition, enabling evaluation of fine-grained language sensitivity.

After constructing both datasets, we forward each pair  $(s^+, s^-)$  through the model and compute the log-probability of the corresponding output sequences.

## C.2. Main Experiment

We provide detailed implementation specifications for the OSPO framework. Table 7 summarize the training configurations used in Step 4 for the three main experimental models: Janus-Pro-7B (Chen et al. 2025) Unitok-MLLM-7B (Ma et al. 2025a), and Janus-1.3B (Wu et al. 2025), respectively.

## D. Additional Analysis

To evaluate the effectiveness of OSPO, we conduct comprehensive ablation studies and analyses. We begin by exam-

ining the effects of iterative training, test-time scaling, and data scaling. Subsequently, we compare the self-rewarding model with an external VQA model to assess the potential risk of confirmation bias during self-improving process when using the self- model as a reward estimator. Confirmation bias refers to the tendency of a model to reinforce its own prior outputs, potentially leading to self-reinforcing errors during self-improvement. This analysis aims to determine whether the self-improving model can provide reliable reward signals without external feedback.

### D.1. Effect of Iterative Training

As shown in Table 8, we present the progression of model performance on T2ICompBench++ across training iterations. The results indicate that the OSPO framework leads to steady and meaningful improvements in text-image alignment across a wide range of compositional categories, with a particularly notable improvement observed after the first iteration.

### D.2. Effect of Test-time Scaling

We introduce Test-Time Scaling (TTS) as an inference-time extension of the OSPO framework, enabling faithful image selection without requiring external supervision. This extension enables OSPO not only to learn better alignment between an input text and an output image during training, but also to self-judge the alignment at the test time. To evaluate the effectiveness of TTS, we compare it against a standard

| Method               | T2ICompBench++ |             |             |             | GenEval     |
|----------------------|----------------|-------------|-------------|-------------|-------------|
|                      | A              | L           | NS          | C           |             |
| Janus-Pro + OSPO     | 0.75           | 0.44        | 0.32        | 0.42        | 0.82        |
| w/ Beam Search       | 0.76           | 0.45        | 0.32        | 0.41        | 0.80        |
| w/ Test-Time Scaling | <b>0.77</b>    | <b>0.46</b> | <b>0.32</b> | <b>0.42</b> | <b>0.85</b> |

Table 9: Performance comparison of different inference-time configurations.

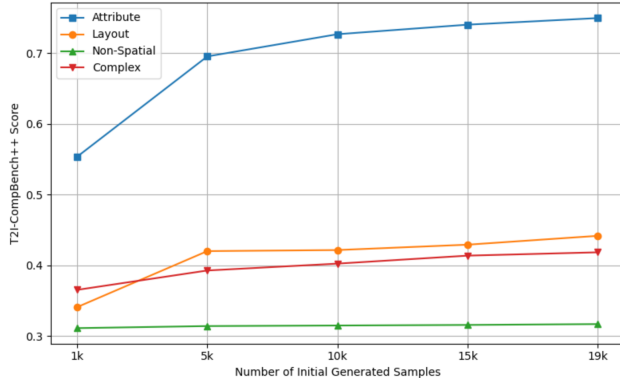


Figure 6: Effect of initially generated data size on T2I-CompBench++ performance.

decoding method based on multiple token sampling, Beam Search, which selects an image with the highest likelihood from the model’s output distribution (with a beam size of 5). In contrast, our TTS strategy leverages Decompositional VQA to score the alignment between the prompt and each generated image. Specifically, we apply TTS by selecting one image out of five candidates for T2I-CompBench++, and four out of ten for GenEval, based on the highest VQA scores, as GenEval’s evaluation protocol requires four images per prompt. Notably, as shown in Table 9, the Decompositional VQA-based strategy originally employed as the reward signal in our OSPO framework achieves the highest performances across benchmarks, further validating its effectiveness for inference-time image selection.

### D.3. Impact of Initial Prompt Data Size Generated from Step 1

To assess the impact of dataset size in the initial prompt generation stage (Step 1), we vary the number of sampled prompts and follow the remaining steps as originally defined. As shown in Figure 6, increasing the dataset size consistently improves overall performances. Specifically For the Attribute and Layout categories, performance improved significantly when the dataset size increased from 1k to 5k, and then showed marginal gains with further increases. Specifically, for the Attribute and Layout categories, performance improved significantly as the dataset size increased from 1k to 5k, with only marginal gains beyond that point. In the Attribute category, the score rose from 0.55 at 1k to 0.70 at 5k, indicating a substantial improvement, and further increased to 0.75 at 19k. In the Layout category, the score improved

| Metric                | Category of Data |      |      |      | Average |
|-----------------------|------------------|------|------|------|---------|
|                       | A                | L    | NS   | C    |         |
| Hit Rates             | 0.91             | 0.80 | 0.85 | 0.90 | 0.87    |
| Mean VQA Score (Self) | 0.77             | 0.54 | 0.71 | 0.83 | 0.68    |
| Mean VQA Score (Qwen) | 0.67             | 0.38 | 0.50 | 0.67 | 0.53    |

Table 10: Comparison of hit rate and VQA score across categories. The hit rate measures answer agreement between the self-rewarding model and the advanced model, while the VQA score reflects the semantic fidelity of each image as assessed by visual question answering. Higher values indicate better alignment.

| VQA Model | T2ICompBench++ |             |             |             | DPGBench     | GenEval     |
|-----------|----------------|-------------|-------------|-------------|--------------|-------------|
|           | A              | L           | NS          | C           |              |             |
| Self      | 0.75           | 0.44        | <b>0.32</b> | <b>0.42</b> | 85.34        | <b>0.82</b> |
| Qwen      | <b>0.77</b>    | <b>0.45</b> | <b>0.32</b> | 0.42        | <b>85.74</b> | 0.81        |

Table 11: Performance comparison of models trained with different VQA reward supervision.

from 0.34 at 1k to 0.42 at 5k, followed by a slight increase to 0.44 at 19k. For the Non-Spatial and Complex Composition categories, scores also improved with larger dataset sizes, but the gains were relatively modest. This is likely due to the CLIP-T score’s low sensitivity within its scoring range, as noted in the Main Results. In the Non-Spatial category, the score increased only slightly from 0.31 at 1k to 0.32 at 19k. In the Complex category, the score improved from 0.37 at 1k to 0.42 at 19k.

### D.4. Confirmation Bias

In the OSPO framework, single MLLM serves both as a generator and a reward estimator, following the self-improving principle of using internal feedback to guide learning. In this section, we evaluate the validity of using the MLLM itself, specifically Janus-Pro-7B, as a reward estimator within the framework, by comparing its reward outputs with those of a strong vision-language model, Qwen-VL-2.5-7B (Bai et al. 2025).

Table 10 presents the differences in VQA scores  $s$  for the same question and image, computed using the following equation:

$$s(v, q) = p(\text{"yes"} | v, q) - p(\text{"no"} | v, q), \quad (8)$$

where  $q$  is a visual question evaluating the semantic fidelity of the image with respect to its text prompt, and  $v$  is the generated image. The comparison is made between the self-rewarding model and a stronger vision-language model (Qwen-VL-2.5-7B). In addition, we report the hit rate, which measures the proportion of matching answers between the self-model and the stronger model.

As shown in Table 10, the hit rates are consistently high across categories, reaching approximately 85%. This indicates that the self-model aligns closely with the strong VQA model in terms of VQA performance, suggesting that its VQA scores can be considered reasonably reliable. However, the largest discrepancy appears in the Layout category,

| Prompt                                    | Self          |              | External Model (Qwen) |              |
|---|---------------|--------------|-----------------------|--------------|
|   | Winning Image | Losing Image | Winning Image         | Losing Image |
| A <u>green</u> fish bowl                  |               |              |                       |              |
| A <u>navy</u> cat and a <u>purple</u> sky |               |              |                       |              |
| A cat <u>above</u> a tree                 |               |              |                       |              |
| Four <u>cats</u>                          |               |              |                       |              |

Figure 7: (Left) Training data examples filtered from the self-rewarding model. (Right) Training data examples filtered from an external model (Qwen-VL-2.5-7B).

where both the self-model and many MLLMs commonly struggle due to challenges in spatial reasoning. Moreover, a comparison of mean VQA scores reveals that the self-rewarding model consistently assigns higher scores than the stronger model. Figure 7 shows example instances from the datasets filtered and selected based on the distinct VQA results produced by each reward model.

The VQA outputs from the self-rewarding model are not fully consistent with those of the stronger model, leading to differences in the resulting data filtering process. To evaluate whether such differences affect downstream training performance, we conducted a controlled experiment. The results demonstrate that the models trained on datasets filtered<sup>3</sup> by each VQA scorer achieve nearly identical performances across all benchmarks, as shown in Table 11. These results indicate that using the model itself as a reward model for VQA-based data filtering is not significantly affected by potential confirmation bias when acting as its own reward model. In this context, confirmation bias refers to the tendency of the model to reinforce its prior outputs by favoring responses that align with its own predictions, which can lead to self-reinforcing errors.

## E. Data Examples

In this section, we present representative examples generated throughout our framework.

<sup>3</sup>Only the filtering process based on VQA scores differs across models. The selection process is uniformly performed based on the training model’s uncertainty.

| Prompt   | w/ Densification |              | w/o Densification |              |
|--|------------------|--------------|-------------------|--------------|
|  | Winning Image    | Losing Image | Winning Image     | Losing Image |
| A <u>blue</u> house and a <u>purple</u> cat  |                  |              |                   |              |
| Three <u>apples</u> and <u>one</u> banana  |                  |              |                   |              |
| A person <u>on the left</u> of a river   |                  |              |                   |              |
| Two of friends are <u>playing a game of basketball</u> in the park during a sunny afternoon. |                  |              |                   |              |

Figure 8: (Left) Training data examples whose images are generated from densified prompts. (Right) Training data examples whose images are generated from non-densified (original) prompts.

**E.1. Prompt Densification** Tables 12 and 13 show the initial positive prompt along with three types of hard negative prompts obtained through perturbation. The final column shows the corresponding densified prompts derived from each short positive and negative prompt.

**E.2. Comparison between images generated from the original prompt and the densified prompt** The Figure 8 shows examples of two images: one generated from the original prompt and the other from the corresponding densified prompt. Although both prompts are intended to convey the same semantic content, the image generated from the densified prompt aligns more accurately with the intended meaning.

## F. Prompt Templates

We leverage the In-Context Learning (ICL) (Dong et al. 2022) capabilities of MLLMs during the processes of Initial Prompt Generation, Hard Preference Pair Generation, and Filtering and Selection. Specifically, we first generate original prompts corresponding to four categories—Attribute, Layout, Non-Spatial, and Complex Composition. Using these original prompts, we construct negative prompts, which are then used to produce dense prompts. During the Filtering and Selection step, we also generate VQA prompts to perform Decompositional VQA, again leveraging the ICL capabilities of the MLLMs.

| Positive(=initial) Prompt     | Densified Positive Prompt   |
|-------------------------------|---|
| A blue house and a purple cat | A quaint, blue-painted house with a charming porch and a cheerful purple cat lounging on the wooden steps, watching a soft spring breeze rustle the nearby wildflowers.                         |
| A blue house and a purple cat | A charming blue house with a white picket fence and a lush garden, nestled beside a serene purple cat with shimmering lavender fur, sitting in the garden under the warm glow of a setting sun. |
| A blue house and a purple cat | A charming blue house with a curved roofline and a bright purple cat lounging lazily on the soft grass in the front yard, its fur shimmering in the warm afternoon sun.                         |

Table 12: Examples of densified positive prompts.

| Perturbation Type | Negative Prompt                              | Densified Negative Prompt   |
|-------------------|--|---|
| Swap              | A <u>purple</u> house and a <u>blue</u> cat  | A quaint, <u>purple</u> -painted house with a charming porch and a cheerful <u>blue</u> cat lounging on the wooden steps, watching a soft spring breeze rustle the nearby wildflowers.                    |
| Drop              | A <u>blue</u> house                          | A charming <u>blue</u> house with a white picket fence and a lush garden, under the warm glow of a setting sun.   |
| Replace           | A <u>green</u> house and a <u>yellow</u> cat | A <u>cozy</u> , <u>green</u> -painted house with a <u>welcoming</u> <u>yellow</u> cat perched on the wooden steps, gazing at a warm summer sun filtering through the vibrant leaves of a nearby oak tree. |

Table 13: Examples of prompt perturbations (negative prompts) and their corresponding densified prompts, based on the pairing positive prompt: “A blue house and a purple cat.” Underline indicates the part of the caption that is semantically different from the positive prompt.

| Initial Prompt Generation Template  |
|---|
| <b>System Prompt:</b> You are an assistant dedicated to generating natural prompts that contain subjects and objects by using color words such as red, orange, yellow, green, blue, navy, purple. Do not repeat any previously used colors in subsequent prompts. |
| <b>User:</b> Generate a prompt that contains subjects and objects by using color words. Except for the color generated before, do not use the same color.   |
| <b>Assistant:</b> Prompt: a blue bench and a green car.; Concepts and relations: blue bench, green car; Relation: (bench, blue), (car, green)   |
| <b>User:</b> Generate a prompt that contains subjects and objects by using color words. Except for the color generated before, do not use the same color.   |
| <b>Assistant:</b> Prompt: a red elephant and a white grass.; Concepts and relations: red elephant, white grass; Relation: (elephant, red), (grass, white)   |
| <b>User:</b> Generate a prompt that contains subjects and objects by using color words. Except for the color generated before, do not use the same color.   |

| generated before, do not use the same color.  |
|---|
| <b>Assistant:</b> Prompt: a yellow pendant and an orange apple.; Concepts and relations: yellow pendant, orange apple; Relation: (pendant, yellow), (apple, orange) |
| <b>User:</b> Generate a prompt that contains subjects and objects by using color words. Except for the color generated before, do not use the same color.           |
| <b>Assistant:</b>   |
| Hard Negative Prompt Generation Template  |
| <b>System Prompt:</b> You are a helpful assistant that generates object-level contrastive prompts by following four steps.  |
| Step 1. Identify all objects in the prompt.   |
| Step 2. Identify all object-attribute bindings in the prompt.   |
| Step 3. Apply one of the following transformations to the given prompt: (1) ‘replace’ an attribute or object with another plausible one, (2) ‘swap’ two             |

attributes or objects, or (3) ‘drop’ an attribute or object.

Step 4. Generate contrastive prompts based on the transformations.

Always ensure the output has opposing or conflicting semantics compared to the input. Do not just reorder or repeat the input.

**User:** a blue bench and a red car

Generate object-level contrastive prompts by applying the following transformation: ‘replace’. Let’s think step by step.

**Assistant:** Step 1. Objects: bench, car

Step 2. Attribute Bindings: ['blue', 'bench'], ['red', 'car']

Step 3. Transformation: ‘replace’; Transformed Attributes: ['white', 'bench'], ['green', 'car']

Step 4. Contrastive Prompt: a white bench and a green car

**User:** a rubber tire and a wooden desk

Generate object-level contrastive prompts by applying the following transformation: ‘swap’. Let’s think step by step.

**Assistant:** Step 1. Objects: tire, desk

Step 2. Attribute Bindings: ['rubber', 'tire'], ['wooden', 'desk']

Step 3. Transformation: ‘swap’; Transformed Attributes: ['wooden', 'tire'], ['rubber', 'desk']

Step 4. Contrastive Prompt: a wooden tire and a rubber desk

**User:** a oblong sweet potato and teardrop mango

Generate object-level contrastive prompts by applying the following transformation: ‘drop’. Avoid changing the original attribute bindings of the objects that are not dropped. Let’s think step by step.

**Assistant:** Step 1. Objects: sweet potato, mango

Step 2. Attributes Bindings: ['oblong', 'sweet potato'], ['teardrop', 'mango']

Step 3. Transformation: ‘drop’; Transformed Attributes: ['teardrop', 'mango']

Step 4. Contrastive Prompt: a teardrop mango

**User:** {input\_prompt}

Generate object-level contrastive prompts by applying the following transformation: {perturbation\_type}. Let’s think step by step.

**Assistant:**

## Dense Prompt Generation Template

**System Prompt:** You are an expert prompt engineer for text-to-image models. Your job is to take short and vague prompts and expand them into detailed, descriptive, and unambiguous prompts suitable for

high-quality image generation.

Focus on using full sentences and include visual attributes such as objects, colors, texture, shape.

Avoid abstract or subjective words and instead use concrete and visual language.

Do not invent unrelated concepts; only expand and clarify the given prompt.

Follow these steps:

Step 1. Extract all objects and their visual attributes from Prompt 1.

Step 2. For Prompt 1, write a long, rich description that includes all identified objects and attributes from Step 1.

Step 3. Extract all objects and their visual attributes from Prompt 2.

Step 4. For Prompt 2, write a long, rich description that includes all identified objects and attributes from Step 3.

Ensure both outputs share a similar global context or scene.

**User:** Prompt 1: A large watermelon

Prompt 2: A small watermelon

Generate dense, detailed prompts. Ensure both outputs share a similar global context or scene but have different object-attribute bindings. Let’s think step by step.

**Assistant:**

Step 1. Prompt 1 Object Bindings: watermelon-[‘large’]

Step 2. Prompt 1 Dense: A large, ripe watermelon with deep green rinds and faint striping rests heavily in a handwoven wicker basket placed on the grass under dappled sunlight beside a weathered garden shed.

Step 3. Prompt 2 Object Bindings: watermelon-[‘small’]

Step 4. Prompt 2 Dense: A small, round watermelon with bright green skin and subtle mottling sits neatly in a handwoven wicker basket placed on the grass under dappled sunlight beside a weathered garden shed.

**User:** Prompt 1: A peach tree and a square computer keyboard

Prompt 2: An orange tree and a square keyboard

Generate dense, detailed prompts. Ensure both outputs share a similar global context or scene but have different object-attribute bindings. Let’s think step by step.

**Assistant:**

Step 1. Prompt 1 Object Bindings: tree-[‘peach’]; keyboard-[‘square’, ‘computer’]

Step 2. Prompt 1 Dense: A peach tree in full bloom stands beside a sleek, square-shaped computer keyboard resting on a polished wooden desk, with soft morning sunlight streaming through the windows of a quiet home office.

Step 3. Prompt 2 Object Bindings: tree-[‘orange’];

keyboard-[‘square’]

Step 4. Prompt 2 Dense: An orange tree with lush green leaves and dangling fruit stands beside a sleek, square-shaped computer keyboard resting on a polished wooden desk, with soft morning sunlight streaming through the windows of a quiet home office.

**User:** Prompt 1: A long in length elephant and a teal owl

Prompt 2: A short elephant and a blue owl  
Generate dense, detailed prompts. Let’s think step by step.

**Assistant:**

Step 1. Prompt 1 Object Bindings: elephant-[‘long in length’]; owl-[‘teal’]

Step 2. Prompt 1 Dense: A long-bodied elephant with weathered gray skin trudging slowly through a misty jungle path, accompanied by a serene teal owl perched on a mossy branch overhead, its feathers glimmering in the filtered morning light.

Step 3. Prompt 2 Object Bindings: elephant-[‘short’]; owl-[‘blue’]

Step 4. Prompt 2 Dense: A short, stocky elephant with wrinkled gray skin navigating a misty jungle path, accompanied by a curious blue owl perched on a mossy branch overhead, its feathers catching flecks of golden morning light.

**User:** Prompt 1: {base\_input\_prompt}

Prompt 2: {negative\_input\_prompt}  
Generate dense, detailed prompts. Ensure both outputs share a similar global context or scene but have different object-attribute bindings. Let’s think step by step.

**Assistant:**

## VQA Prompt Generation Template

**System Prompt:** You are an assistant dedicated to transforming a sentence into several questions. You should first divide it into simple concepts and relations, and then provide the corresponding questions. Avoid using pronouns, such as he, she, it, and they.

**User:** A white harp and a rust soup.

**Assistant:** Concepts and relations: a white harp, a rust soup; Questions: Is there a white harp? Is there a rust soup?

**User:** A quarter circle lily and a hexagon mirror.

**Assistant:** Concepts and relations: a quarter circle lily, a hexagon mirror; Questions: Is there a quarter-circle lily? Is there a hexagon mirror?

**User:** Shiny mop and metal key holder.

**Assistant:** Concepts and relations: a shiny mop, a metal key holder; Questions: Is there a shiny mop? Is there a metal key holder?

**User:** {input\_prompt}

**Assistant:**

## G. Qualitative Examples

We present additional visual examples to qualitatively and intuitively compare each baseline (Janus-Pro-7B, UniTok-MLLM-7B, and Janus-1.3B) with the corresponding results after applying OSPO. Figures 9 and 10 present comparisons between Janus-Pro-7B and Janus-Pro-7B + OSPO on T2I-CompBench++, GenEval, and DPGBench. Similarly, Figures 11 and 12 show comparisons between UniTok-MLLM-7B and UniTok-MLLM-7B + OSPO on the T2I-CompBench++, GenEval, and DPGBench. Figures 13 and 14 present comparisons between Janus-1.3B and Janus-1.3B + OSPO on T2I-CompBench++, GenEval, and DPGBench as well.

As shown in the results, the baseline models Janus-Pro-7B, UniTok-MLLM-7B, and Janus-1.3B often fail to follow the prompt accurately, exhibiting object omissions, incorrect attribute bindings, and overall misalignment between the text prompt and the generated image. In contrast, applying the OSPO method leads to improved alignment, with models better preserving object presence and correctly binding attributes. These results highlight the effectiveness of OSPO in mitigating object-level hallucinations.

|                      | Janus-Pro  | Janus-Pro + OSPO (ours) | Janus-Pro  | Janus-Pro + OSPO (ours) |
|----------------------|--|-------------------------|--|-------------------------|
| <b>T2I-Compbench</b> |  |                         |  |                         |
| Attribute            |  |                         |  |                         |
|                      | A <u>black</u> jacket and a <u>brown</u> hat                                 |                         | A book <u>in front of</u> a candle   |                         |
| Non-spatial          |  |                         |  |                         |
|                      | The woodcarver is creating a <u>sculpture of a bird</u> from a block of wood |                         | The <u>colorful</u> hot air balloon floated near the <u>dark grey</u> storm clouds |                         |
| <b>GenEval</b>       |  |                         |  |                         |
|                      |  |                         |  |                         |
|                      | A photo of <u>three cups</u>   |                         | A photo of <u>a pink skateboard</u> and a <u>black train</u>                       |                         |
|                      |  |                         |  |                         |
|                      | A photo of <u>a green cup</u> and <u>a red pizza</u>                         |                         | A photo of a bed <u>right of</u> a sport ball                                      |                         |

Figure 9: Additional Qualitative results of Janus-Pro-7B (Chen et al. 2025) and Janus-Pro-7B + OSPO on T2I-CompBench++ (Huang et al. 2025) and GenEval (Ghosh, Hajishirzi, and Schmidt 2023).

| Janus-Pro       | Janus-Pro + OSPO (ours) |
|-----------------|-------------------------|
| <b>DPGBench</b> |                         |
|                 |                         |

A worn piece of luggage placed beside a metal spoon, both lying atop an aged, dusty table. The dim light of the moon barely illuminates the objects, revealing their outlines in the quiet darkness of midnight. Shadows stretch across the table's surface, enhancing the stillness of the nocturnal scene.

A surreal lunar landscape unfolds with the iconic Great Pyramids and the Sphinx, all replicated in meticulous detail on the moon's dusty, grey surface. In the foreground, the silhouette of an astronaut, clad in a pearly white spacesuit, is captured from behind, gazing upon the ancient wonders. Above this otherworldly scene, the Earth hangs majestically in the dark expanse of space, its blue and white visage a stark contrast to the barren moonscape.

A detailed sketch of a space shuttle, rendered in the intricate, technical style reminiscent of Leonardo da Vinci's famous drawings. The shuttle is depicted with numerous annotations and measurements, showcasing its complex design and structure. The paper on which it is drawn has an aged, yellowed appearance, adding to the historical feel of the artwork.

Figure 10: Additional Qualitative results of Janus-Pro-7B (Chen et al. 2025) and Janus-Pro-7B + OSPO on DPGBench (Hu et al. 2024).

|                      | UniTok  | Unitok<br>+ OSPO (ours) | UniTok   | Unitok<br>+ OSPO (ours) |
|----------------------|---|-------------------------|--|-------------------------|
| <b>T2I-Compbench</b> |   |                         |  |                         |
| Attribute            |   |                         |  |                         |
|                      | A bathroom with <u>beige</u> tile and a <u>white</u> toilet |                         | A turtle <u>behind</u> a pig   |                         |
| Non-spatial          |   |                         |  |                         |
|                      | A <u>boat</u> is sailing on a lake                          |                         | The <u>soft</u> , <u>plush</u> texture of the <u>teddy</u> <u>bear</u> was a comforting companion for the child at bedtime |                         |
| <b>GenEval</b>       |   |                         |  |                         |
|                      |   |                         |  |                         |
|                      | A photo of a <u>white</u> pizza and a <u>green</u> umbrella |                         | A photo of vase <u>right</u> of a horse  |                         |
|                      |   |                         |  |                         |
|                      | A photo of <u>three</u> cows                                |                         | A photo of a <u>white</u> wine glass and a <u>brown</u> giraffe  |                         |

Figure 11: Additional Qualitative results of UniTok-MLLM-7B (Ma et al. 2025a) and UniTok-MLLM-7B + OSPO on T2I-CompBench++ (Huang et al. 2025) and GenEval (Ghosh, Hajishirzi, and Schmidt 2023).

| UniTok          | Unitok<br>+ OSPO (ours) |
|-----------------|-------------------------|
| <b>DPGBench</b> |                         |
|                 |                         |

In the fading light of late afternoon, a scene unfolds in the autumn park, where a pair of worn brown boots stands firm upon a bed of fallen orange leaves. Attached to these boots are two vibrant blue balloons, gently swaying in the cool breeze. The balloons cast soft shadows on the ground, nestled among the trees with their leaves transitioning to auburn hues. Nearby, a wooden bench sits empty, inviting passersby to witness the quiet juxtaposition of the still footwear and the dancing balloons.

Three perfectly shaped dumplings, with their pleats meticulously crimped, sit in solitude on a reflective glass surface which captures their image under the soft glow of a moonlit night. The large mirror is resting against a wall with a faint pattern, amplifying the quietude of midnight. The room is hushed, with the only movement being the gentle shift of shadows as the night deepens, highlighting the stillness of the scene.

In the midst of a vibrant garden, a cylindrical green cup stands alone on a stone path, its surface reflecting the bright afternoon sunlight. The cup, with a smooth finish, is surrounded by blossoming flowers and lush greenery. The shadows of nearby plants dance on the cup as gentle breezes sway their leaves.

Figure 12: Additional Qualitative results of UniTok-MLLM-7B (Ma et al. 2025a) and UniTok-MLLM-7B + OSPO on DPGBench (Hu et al. 2024).

|                      | Janus   | Janus<br>+ OSPO (ours)  | Janus   | Janus<br>+ OSPO (ours)  |
|----------------------|---|---|---|---|
| <b>T2I-Compbench</b> |   |   |   |   |
| Attribute            |    |    |  |  |
|                      | A <u>blue</u> duck and a <u>yellow</u> pond   |   | A cat <u>on the left of</u> a lamp  |   |
| Non-spatial          |    |    |  |  |
|                      | A horse <u>is galloping</u> in a meadow   |   | The <u>black chair</u> <u>is on top of</u> the <u>blue rug</u>                    |   |
| <b>GenEval</b>       |   |   |   |   |
|                      |  |  |   |   |
|                      | A photo of <u>a stop sign</u> and <u>a dog</u>                                      |   | A photo of <u>two</u> toothbrushes  |   |
|                      |  |  |   |   |
|                      | A photo of a couch <u>below</u> a cup   |   | A photo of a <u>pink</u> skateboard and a <u>black</u> train                      |   |

Figure 13: Additional Qualitative results of Janus-1.3B (Wu et al. 2025) and Janus-1.3B + OSPO on T2I-CompBench++ (Huang et al. 2025) and GenEval (Ghosh, Hajishirzi, and Schmidt 2023).

| Janus  | Janus<br>+ OSPO (ours)   |
|--|--|
| <b>DPGBench</b>  |  |
|    |   |
|  | A <u>traditional Venetian mask</u> with intricate designs and feather embellishments is placed on a <u>polished wooden table</u> . Next to the mask, there sits a substantial <u>golden trophy</u> , <u>shining with reflected light</u> , its surface etched with small, detailed engravings. The table and its <u>prestigious items</u> are set against a deep sepia-toned backdrop that enhances the objects' visual appeal.  |
|   |    |
|  | A <u>vibrant yellow rabbit</u> , its fur almost glowing with cheerfulness, bounds <u>energetically across a sprawling meadow</u> dotted with a constellation of wildflowers. The creature's sizeable, <u>red-framed glasses</u> slip comically to the <u>tip of its nose</u> with each jubilant leap. As the first rays of <u>sunlight cascade over the horizon</u> , they illuminate the dew-draped blades of grass, casting the <u>rabbit's exuberant shadow</u> against the fresh green canvas.   |
|  |   |
|  | A picturesque scene where the expansive blue sky arches over a <u>stationary train</u> , which sits on a set of tracks that cut a straight line through the landscape. The train engine is an unusual sight, <u>covered in tufts of green grass</u> , creating a contrast between machinery and nature. In the distance, a <u>mountain looms over the train</u> , imposing its grandeur on the scene. Below the grass-adorned engine, the <u>hard gravel of the track</u> meets the edge of an asphalt road that runs parallel, with <u>more trains in the distance</u> continuing their journey under the vast sky. |

Figure 14: Additional Qualitative results of Janus-1.3B (Wu et al. 2025) and Janus-1.3B + OSPO on DPGBench (Hu et al. 2024).